Ultra-thin flexible polyimide neural probe embedded in a dissolvable maltose-coated microneedle

2014 J. Micromech. Microeng. 24 065015

IOP Publishing Journal of Micromechanics and Microengineering
J. Micromech. Microeng. **24** (2014) 065015 (11pp) doi:10.1088/0960-1317/24/6/065015

Ultra-thin flexible polyimide neural probe embedded in a dissolvable maltose-coated microneedle

Zhuolin Xiang[1,2], Shih-Cheng Yen[1,2,5], Ning Xue[3], Tao Sun[3], Wei Mong Tsang[3], Songsong Zhang[1,3], Lun-De Liao[2], Nitish V Thakor[2,4] and Chengkuo Lee[1,2,5]

[1] Department of Electrical and Computer Engineering, National University of Singapore, 4 Engineering Drive 3, 117576, Singapore
[2] Singapore Institute for Neurotechnology (SiNAPSE), National University of Singapore, 28 Medical Drive, 05-COR, 117456, Singapore
[3] Institute of Microelectronics (IME), Agency for Science, Technology and Research (A*STAR), 11 Science Park Road, Singapore Science Park II, 117685, Singapore
[4] Department of Biomedical Engineering, School of Medicine, Johns Hopkins University, Baltimore, MD 21205, USA

E-mail: shihcheng@nus.edu.sg and elelc@nus.edu.sg

Received 20 February 2014, revised 4 April 2014
Accepted for publication 14 April 2014
Published 14 May 2014

Abstract

The ultra-thin flexible polyimide neural probe can reduce the glial sheath growth on the probe body while its flexibility can minimize the micromotion between the probe and brain tissue. To provide sufficient stiffness for penetration purposes, we developed a drawing lithography technology for uniform maltose coating to make the maltose-coated polyimide neural probe become a stiff microneedle. The coating thicknesses under different temperature and the corresponding stiffness are studied. It has been proven that the coated maltose is dissolved by body fluids after implantation for a few seconds. Moreover, carbon nanotubes are coated on the neural probe recording electrodes to improve the charge delivery ability and reduce the impedance. Last but not least, the feasibility and recording characteristic of this ultra-thin polyimide neural probe embedded in a maltose-coated microneedle are further demonstrated by *in vivo* tests.

Keywords: neural probe, microneedle, dissolvable, maltose, ultra-thin, flexible

(Some figures may appear in colour only in the online journal)

1. Introduction

Implantable arrays of neural probes with microelectrodes have drawn more and more attention for their use in studying brain function since they can simultaneously record signals from different groups of neurons and gather spatiotemporal information regarding complex neural processes. Compared with electroencephalograms or electrocorticograms, implanted neural probes can provide superior spatial resolution and enable recordings in deeper brain structures [1–3]. Implantable neural probes based on microelectromechanical systems technology have taken significant steps forward in the last 40 years. During the 1970s, Wise *et al* took advantage of selective etching technology and reported pioneering work on the first neural probe to interface with neural tissues [4]. Since then, a wide variety of materials used to fabricate miniaturized neural probes have been developed, including silicon [5–8], metals [9, 10], glass [11] and sapphire [12]. Although neural probes with these materials can be shaped precisely and have sufficient strength to penetrate neural tissue, the mechanical mismatch between these stiff substrates and soft tissue [13–15] aggravates

[5] Authors to whom any correspondence should be addressed.

micromotion at the tissue–electrode contact sites, which induces inflammation in the tissue [16, 17]. Even though thin film silicon probes can partially alleviate the mechanical mismatch [18], deformation induced from the presence of localized stress may lead to the rupture of materials. To solve this problem, polymer materials, such as SU-8 [19–23], parylene [24–27], polyimide [28–32], liquid crystal polymer [33] and benzocyclobutent [34], are often employed in creating flexible neural probes. Since these materials are a better match mechanically to the tissue, and deforms as the tissue moves, flexible neural probes made of these materials can prevent the gradual decrease in the signal-to-noise ratio.

Another serious problem for conventional neural probes is that a reactive glial sheath builds up around the probe body after the invasive implantation process [35]. Histological examination of intra-cortical devices has shown that the glial sheath consists of activated microglia, hypertrophied astrocytes [36, 37], meningeal cells and oligodendrocyte precursors [38]. These cells produce extracellular proteins that hinder local neuron regeneration at implantation sites [39]. In addition, the glial sheath will encapsulate the electrodes on the neural probe and modify the extracellular space, as proved by impedance spectroscopy studies [40–42]. The encapsulation will isolate electrodes from the surrounding neural tissue, which will lead to the eventual failure of the electrode's recording ability in chronic recordings [43, 44]. Conventional strategies to reduce the tissue encapsulation problem are surface modification [45, 46] and local drug delivery [47–49]. In 2007, Seymour *et al* showed that modifying neural probe geometry and shrinking the probe size will provide an alternative to minimize the reactive cell responses [50]. The thinner probe shank can reduce microglia reactivity and extracellular protein deposition, while at the same time decreasing the distance to nearby neurons. However, when the thickness of the polymer neural probe shrinks down to diminish the encapsulation problem the neural probe will become extremely flexible. This makes the stiffness of the probe too low to penetrate neural tissue successfully. Stiff backbone layers [26, 51], insertion shuttles [52, 53] and coating biodegradable material [24] have been employed to enhance the structural stiffness of the flexible probes. Among them, the stiff backbone negates the flexibility of the polymer substrate, while insertion shuttles creates a relatively large implanted footprint and a high rupture risk. Coating with biodegradable materials such as silk [54], poly-glycolic acid [55], polyethelene glycol [56] and poly(lactic-co-glycolic) [57] has become a popular approach to improve the stiffness since it is a simple process and does not need any modification of the probe structure.

During the signal recording or stimulation process, the impedance must be lowered to increase electrode sensitivity or to facilitate electric discharge. This step generally increases the dimension of the electrodes as well as the neural probe body, which leads to the loss of signal selectivity and increases tissue damage during insertion. The typical approach of inducing a colloidal metal layer to increase the surface area for a certain geometric area can encounter stability problems. For instance, platinum black when electrodeposited is a porous

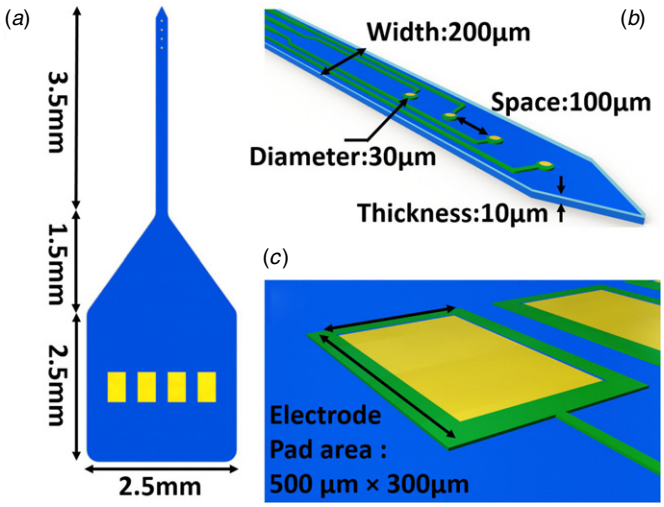

Figure 1. Schematic illustration of the neural probe design.

structure and has low impedance, but it is mechanically fragile and degrades over time [58]. Activated iridium oxide demonstrates excellent charge transfer properties, but its surface is chemically unstable [59]. However, the technique of coating carbon nanotubes (CNTs) on electrodes has been demonstrated to not only decrease impedance and increase charge transfer, but also offer satisfactory stability for long-term brain–machine interface devices [60–62].

In this study, we have developed a fabrication process for ultra-thin flexible polyimide neural probes. Its remarkable flexibility contributes to reduce the stiffness difference between brain tissue and electrodes and minimize the micromotion after implantation. In addition, the whole thickness for the neural probe is only 10 μm. The ultra-thin size prevents growth of the glial sheath on the neural probe body [50]. Moreover, maltose, a biodegradable and biocompatible material, is first employed to be coated on the neural probe to promote its stiffness. To achieve favorable coating uniformity, appropriate stiffness and high reproducibility, we adopt an innovative drawing lithography technology to coat the maltose on the neural probe surface. The coating thickness can be controlled by regulating the temperature. This coated maltose layer transforms the flexible neural probe into a stiff microneedle for successful penetration. It can be dissolved by body fluids several seconds after implantation. In addition, CNT-Au nano-composites are integrated into the ultra-thin flexible neural probe to minimize the interface impedance for better signal quality.

2. Design and fabrication

2.1. Fabrication process

The design of the flexible neural probe is shown in figure 1. The neural probe can be divided into three different sections (figure 1(*a*)). At the widest part, a 2.5 mm × 2.5 mm area allows for easy handling and packaging. This is where the external contact electrodes are located. There are four electrode pads, each with an area of 500 μm × 300 μm (figure 1(*c*)). These dimensions ensure easy connection of the neural probe

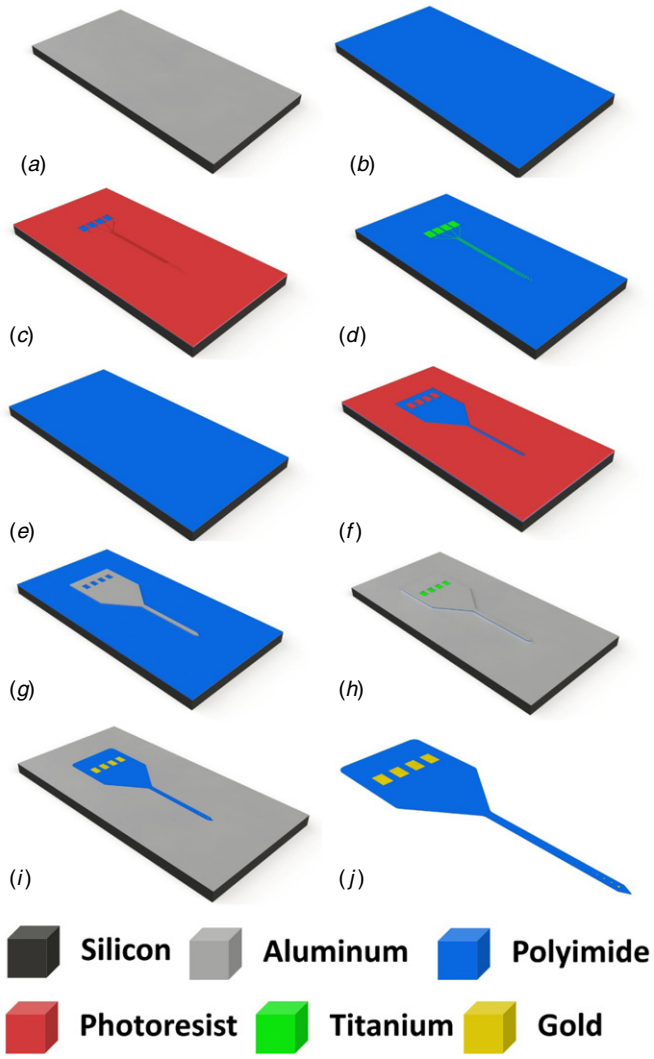

Figure 2. Fabrication process for the ultra-thin flexible polyimide neural probe.

to the flexible printed circuit (FPC) connectors. Then, a 1.5 mm long path is designed to gradually reduce the probe size. The portion of the probe that will be inserted into the tissue is 3.5 mm long in order to reach certain brain areas, with a width of 200 μm and a thickness of 10 μm (figure 1(*b*)). To our knowledge, this 10 μm neural probe is the thinnest polyimide neural probe reported in the literature. This small dimension is expected to alleviate encapsulation problems (caused by scar tissue). At the tip of the neural probe, four round recording contacts with a diameter of 30 μm are placed. The spacing between each two electrodes is 100 μm.

The fabrication procedure follows standard photolithographic and clean room procedures. The detailed process is shown in figure 2. Firstly, a 1 μm thick aluminum (Al) layer was evaporated onto the silicon substrate by physical vapor deposition (figure 2(*a*)). It acted as a sacrificial layer to release the final device from the substrate. Then a 5 μm base layer of polyimide (HD 4110, HD microsystem GmbH, Germany) was spun onto the Si substrate. The base polyimide layer was cured at 300 °C in N_2 for 0.5 h. This baking process is designed to only partially evaporate the water in the polyimide layer. In this way, it would bring a chemically and physically stable surface for further processing, while still leaving some unterminated bonds to attach the top polyimide layer (figure 2(*b*)) [63]. After that, a 7 μm thick layer of photoresist (ma-N 1440, microsystem GmbH, Germany) was spun on the polyimide coated substrate. The photoresist layer was exposed under ultraviolet (UV) light and the electrodes traces were patterned (figure 2(*c*)). A layer of 20 nm titanium (Ti) was deposited by an electron beam evaporator to improve the adhesion of the following metal layers. Then, a 200 nm thick gold conduction layer and a 20 nm thick titanium protection layer were deposited. The electrode pads and contacts could be patterned by a liftoff process in acetone (figure 2(*d*)). Another 5 μm top layer of polyimide was spun onto the processed metal layer. The whole sandwich structure was then cured at 350 °C in N_2 for 0.5 h to complete the imidization process (figure 2(*e*)). Next, a 200 nm thick Al layer was deposited and patterned by using the same liftoff process (figures 2(*f*), (*g*)). This Al layer would be used as a hard mask for the final device etching process. The shape of the electrode pads, contacts and device body were defined by O_2/CF_4 plasma. In the etching process, the undesired polyimide portions were removed by the plasma. The Au electrodes pads and contacts were protected by the top titanium layer while the useful polyimide portions were protected by the Al hard mask (figure 2(*h*)). The plasma etching process was performed by using an electron cyclotron resonance-enhanced reactive ion etcher (gas flows of 10 sccm for O_2 and 10 sccm for CF_4, RF source power of 300 W, with a chamber base pressure of 100 mTorr, resulting in a polyimide etching grate of $\sim$0.1 μm min^{-1}). Then, the Al hard mask and Ti protection layer were removed by Al etchant and Ti etchant respectively (figure 2(*i*)). Since the first Al sacrificial layer was much thicker than the Al hard mask (1 μm for Al sacrificial layer and 200 nm for the Al hard mask), the Al etching time was controlled to only remove Al hard mask. In this way, the whole device was still on the substrate. Then, an anodic dissolution was employed to remove the Al sacrificial layer to release the final devices (figure 2(*j*)). The conventional approach to remove the sacrificial layer is wet etching. However, the residue stress leads to the released thin film structure being deformed [64]. The anodic metal dissolution not only can ensure a flat released planar structure but also is significantly faster than the traditional wet etching approach [65]. The detailed releasing process is shown here. The wafer was immersed in a 2 M NaCl solution and connected to an external positive terminal of a voltage source at 1 V. A platinum (Pt) mesh electrode was connected to the negative terminal. A magnetic stir bar was also put inside the solution to keep a uniform NaCl concentration. After around 20 min, the exposed portions of the Al sacrificial layer were removed and only the covered portions of the Al sacrificial layer were left. Since the contact area between the Al sacrificial layer and the NaCl solution has decreased, the current dropped and the Al etching rate was greatly reduced. Thus, the voltage was then increased to 20 V to speed up the releasing process. After around 1 h, the whole Al sacrificial layer could be removed and the final device could be released (figure 3).

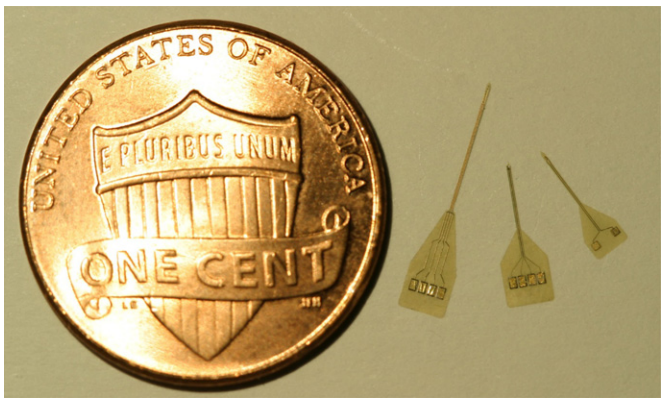

Figure 3. Released ultra-thin flexible neural probe.

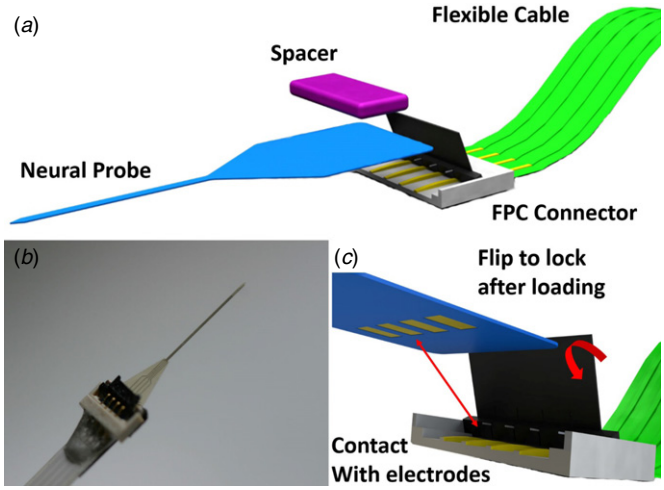

Figure 4. Illustration of the packaging for the probe.

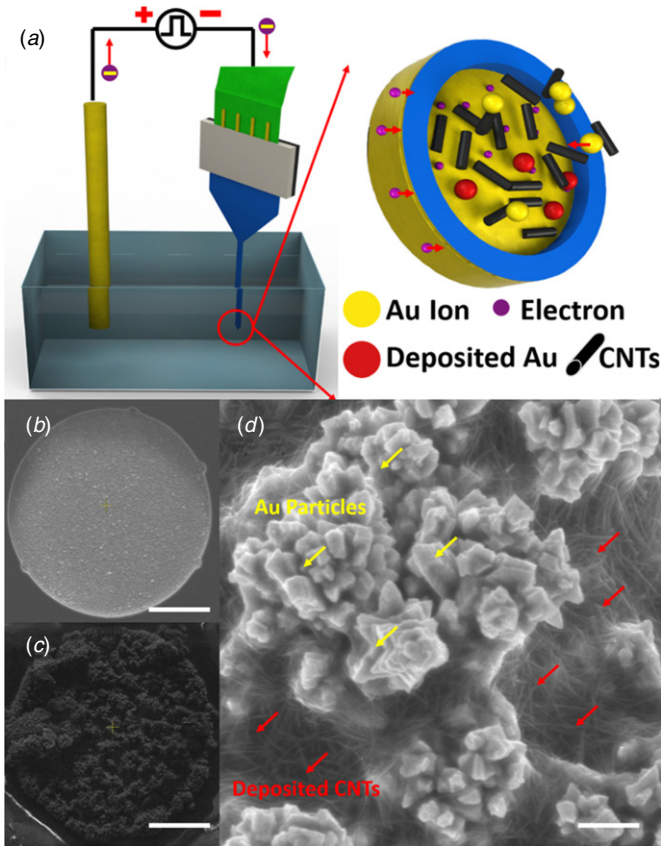

Figure 5. (*a*) Schematic of the setup for the CNT coating. (*b*) Au recording contacts without CNT coating (scale bar is 10 μm). (*c*) Au recording contacts with CNT coating (scale bar is 10 μm). (*d*) Zoomed-in image to show electroplated CNTs and Au particles on the contacts (scale bar is 500 nm).

2.2. Assembling

In order to perform the characterization of the neural probe to obtain data from *in vitro* and *in vivo* tests, electrical interconnections need to be set up between the electrode pads on the flexible substrate and terminals on the measurement equipment. However, it has been reported that there are serious implementation problems if conventional wire bonding technology is to be used [66]. Generally, during the bonding process, the electrodes pads on the flexible substrate will delaminate due to the poor metal/polymer adhesion strength [67]. To solve the problem, isotropic conductive glue and anisotropic conductive films are normally adopted to create the electrical interconnections [68]. However, these processes are time consuming, need precise alignment, and are thus not effective.

In this study, we used a simple FPC connector (FH19SC-6S-0.5SH. Hirose Electric Co. Ltd Japan) to package the final device. Figure 4(*a*) shows a schematic overview of the packaging method. Firstly, the FPC connector was integrated with a flexible cable by the normal soldering approach. Then, the rear of the neural probe was inserted into the groove on the FPC connector. Since the geometry and dimension of our neural probe was specially designed to match the connector, the probe body would be fixed in the horizontal direction. Moreover, electrode pads on the probe could align perfectly with the electrode pins on the FPC connector. After that, a 300 μm thick spacer, which had the same thickness as the vertical spacing in the FPC connector groove, was loaded on top of the probe. Since the total thickness of the inserted spacer and probe body was a little bit larger than the spacing in the groove, when the top cap was flipped over to clamp the spacer, a tiny spring inside the FPC connector would be compressed and the probe could be locked in the perpendicular direction (figure 4(*c*)). Meanwhile, the electrode pads on the flexible probe would make contact with the electrode pins on the FPC connector to achieve the electrical interconnection. The final package is shown in figure 4(*b*).

2.3. CNT deposition and maltose coating

A layer of CNTs was coated on the recording contacts to increase the effective surface area and improve charge transfer at the electrode–tissue interface. The electrophoretic deposition technique was employed to deposit the CNT film since it is an automated and high-throughput process that in general produces films with good homogeneity and packing density [69]. The detailed process is shown in figure 5. The multiwall CNTs (Cheap Tubes Inc., US) were first dispersed in a Au electrolyte bath TSG-250 (Transene, US) to form a 1 mg mL^{-1} aqueous solution. Then, the whole solution was sonicated for 2 h to make the CNTs fully suspended in

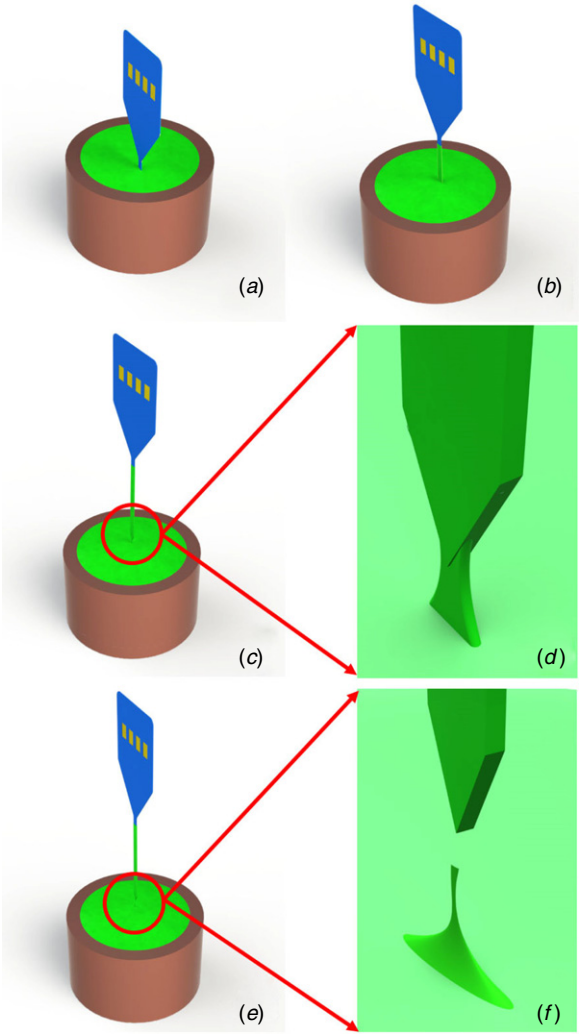

Figure 6. Fabrication process to coat maltose on the flexible neural probe surface by drawing lithography.

the solution. After that, the packaged neural probe and Au wire were connected to the negative and positive terminals of the power supply, respectively. Both the probe tip and the Au wire were then inserted into the solution. A monophasic voltage pulse with 1 V amplitude and 50% duty cycle was applied to the power source. Au ions in the solution, as well as CNTs which absorbed Au ions, migrated to the negative terminals. After absorbing the electrons from the probe contacts, the Au ions were subsequently deposited onto the surface of the recording contacts. The CNTs with a length of 0.5–2 μm and a diameter less than 8 μm could thus be made to adhere to the Au electrode contacts by these ions (figure 5(*a*)). The comparison of an Au electrode contact and a CNT coated contact is shown in figures 5(*b*) and (*c*).

Maltose, a natural biocompatible and biodissolvable material [70], was employed to coat the flexible neural probe surface to form a stiff microneedle. To achieve favorable coating uniformity, appropriate stiffness and high reproducibility, we leveraged an innovative drawing lithography technology to perform the coating process. Drawing lithography technology is a maskless fabrication approach to build 3D structures based on the polymers'

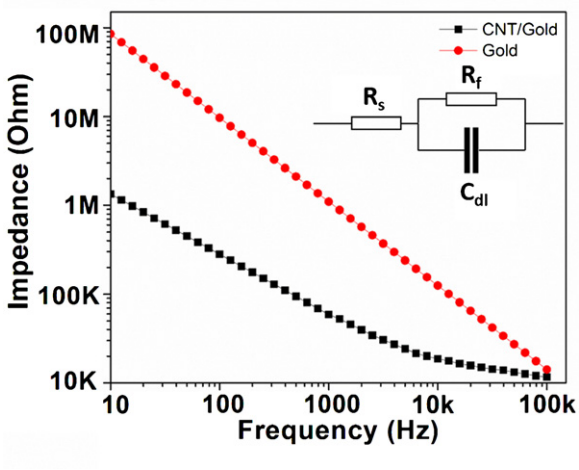

Figure 7. Impedance testing results of Au recording contacts and CNT coated Au recording contacts.

different viscosities under different temperatures [71, 72]. Here, it is applied to coat polymers on the surface of the flexible probes.

As shown in figure 6, the surface maltose coating process was divided into four steps. Firstly, concentrated maltose solution containing methylene blue, which was used for better visibility during the penetration process, was dripped into a small metal container. The container was kept on a hotplate at 140 °C until the water inside vaporized and the maltose turned into the liquid state. The neural probe with an FPC connector was fixed on a precision stage which could control the position of the attached device in three-dimensions. Then, the whole neural probe was immersed into the maltose reservoir by adjusting the precision stage (figure 6(*a*)). In the second step, the neural probe was drawn up and the adhesive maltose was coated on the probe surface (figure 6(*b*)). Thirdly, the temperature of liquid maltose was gradually increased and the neural probe tip was dawn away from the interface between the liquid maltose and air (figure 6(*c*)). Since the maltose liquid is less viscous at higher temperature, the adhesion between the maltose on the probe tip and the surface of the liquid maltose became an individual maltose bridge and shrunk gradually (figure 6(*d*)). Finally, when the temperature rose up to 160 °C, the drawing speed was increased. The end of the shrunk maltose bridge collapsed and formed a sharp tip (figures 6(*e*), (*f*)). In this way, the maltose could be successfully coated on the ultra-thin flexible probe and made into a stiff microneedle for penetration.

3. Characterization

3.1. Impedance spectroscopy

One of the most important considerations of neural recording devices is that the electrodes should be small enough to ensure high selectivity for signals from individual neurons. Impedance measurements were conducted in order to characterize the electrode–electrolyte interface. Two-wire electrochemical impedance spectroscopy measurements were performed with each of the four electrodes versus a

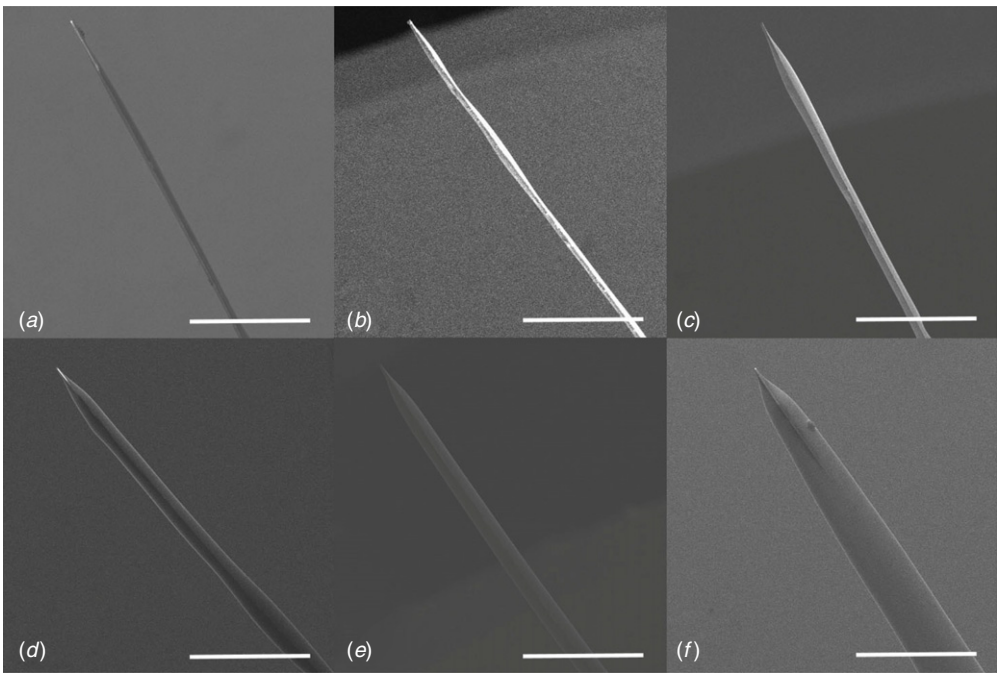

Figure 8. Demonstration of different thickness of maltose coated on the neural probe surface (scale bar is 500 μm).

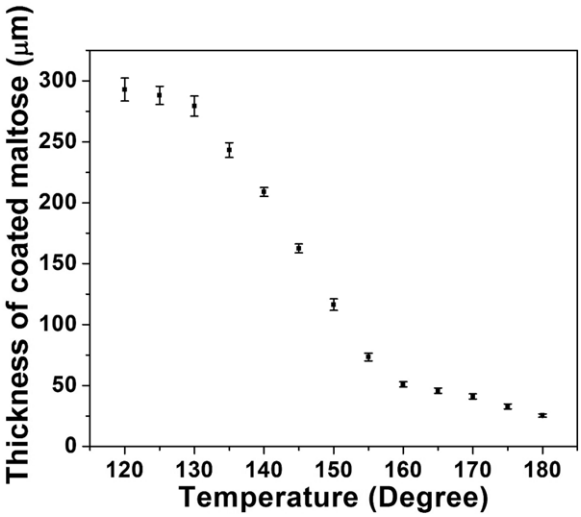

Figure 9. The means and standard errors of the thickness of maltose coated onto the probe under different temperatures.

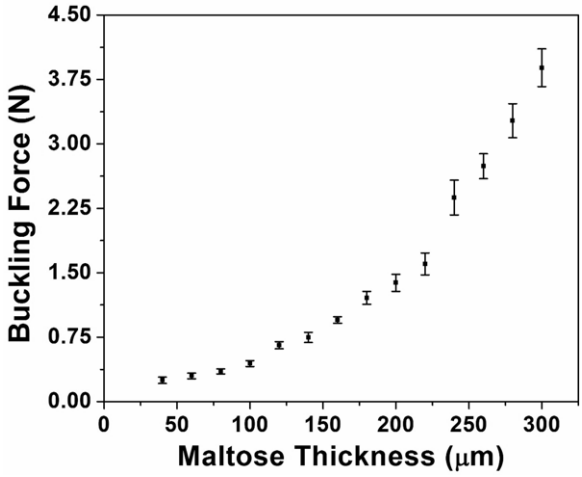

Figure 10. Means and standard errors of the buckling force for microneedles of different thicknesses.

platinum reference electrode by Metrohm Autolab PG Stat 12 Electrochem System (Metrohm Autolab PG. UK). The impedance of both Au recording contacts and CNT coated contacts were checked by measuring the impedance versus frequency from 10 Hz to 100 kHz in a physiological saline solution. Figure 7 shows the testing results. The impedance of both Au contacts and CNT coated contacts showed a considerable dependence on frequency. Meanwhile, the impedance spectroscopy scan showed that the CNT coated electrode contacts exhibited reduced impedances at all the measured frequencies. At the biologically relevant frequency of 1 kHz, the impedance of the Au electrode and the CNT coated electrode were 1.09 MΩ and 59.02 kΩ, respectively. This demonstrated that the interfacial properties of the probes were significantly improved by the CNT. Tsang *et al* attributed this enhancement to the nano-protrusions induced by the coated CNTs [73]. The standard equivalent circuit model for the electrode–electrolyte interface is also shown in figure 7. A constant phase element (for an ideal capacitor $n = 1$) represented the interface between the probe and saline. R_f was regarded as Faradaic impedance while R_s was taken as the spreading resistance of the solution. When the frequency increased from 10 Hz to 100 kHz, the constant phase element decreased as well as the total impedance. Compared with normal Au contacts, the charge injection capability increased on the CNT coated contacts due to the induced nano-protrusions. Since the value C_{dl} was proportional to the charge injection capability, the total impedance of the CNT coated contacts at any frequency was smaller than that of the Au contacts. Thus, this CNT coating technique substantially improved the interfacial properties.

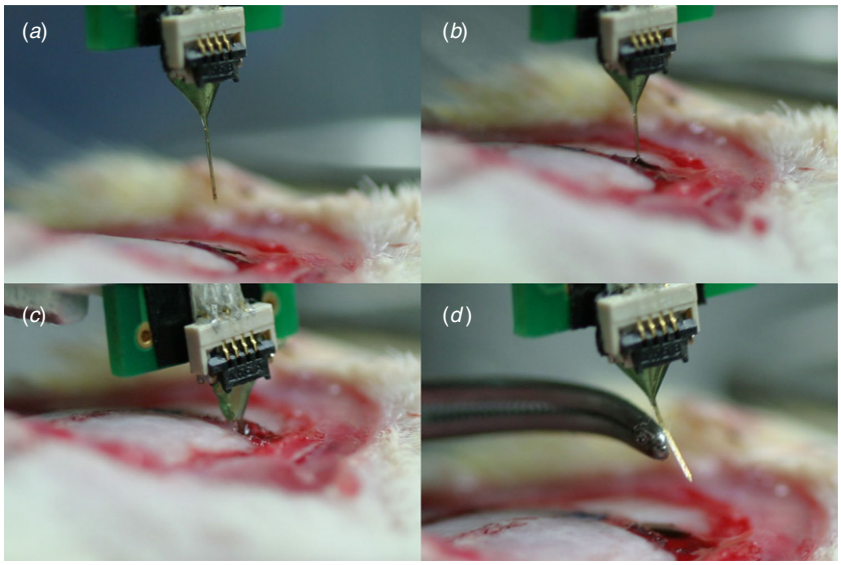

Figure 11. Demonstration that the maltose coated ultra-thin flexible neural probe can successfully penetrate the brain. After the maltose is dissolved by the body fluids, the rigid microneedle becomes a flexible neural probe.

3.2. Thickness of maltose coating

The ultra-thin flexible probe was coated with a layer of maltose to transform it into a stiff microneedle that could be used to penetrate the brain successfully. Maltose was demonstrated to become a liquid at temperatures over its melting point, and the viscosity of this liquid maltose progressively increased with cooling until the glass transition temperature. Further cooling past this temperature causes it to enter the solid state [74]. In this study, by controlling the temperature, we regulated the maltose viscosity to coat a desired thickness of maltose on the ultra-thin flexible probe surface (figure 8). The thickness was measured under various baking temperatures and is shown in figure 9. In general, the microneedle's thickness decreased continuously when the temperature increased. If the baking temperature was less than 130 °C or larger than 160 °C, the coating thickness changed only slightly based on the temperature. It had a more obvious difference when the temperature changed between 130 and 160 °C. This was due to the fact that the viscosity of the maltose solution changed more dramatically in its glass state (between 130 and 160 °C) than in the solid or liquid state. Thus, we can control the thickness of the maltose coating simply by adjusting the baking temperature.

3.3. Mechanical testing

The buckling force of the microneedle was studied by using an ALGOL advanced precision instrument (Japan Instrumentation System Co., Ltd, Japan). The force sensor was vertically mounted on a stationary platform while the maltose coated microneedle was perpendicularly attached to a 3D micromanipulator. Bending force was applied in the vertical direction by adjusting the height of the micromanipulator to make the microneedle tip contact the force sensor. A 3D microscope was used to monitor and capture the deformation and breakage of the microneedles. The vertical displacement of the microneedle tip and the buckling force could be recorded from the precision instrument. Microneedles with the same length of 3.5 mm but different coating thickness were tested. Figure 10 shows the results of the buckling force when microneedles break at the various coating thickness. The thicker the acting of maltose, the stronger the microneedle will be. When the coated thickness is less than 100 μm, all the buckling forces are smaller than 0.5 N. In this regime, the buckling force increases a little when we coat thicker maltose. However, when the microneedle thickness is larger than 120 μm, the buckling force increases sharply. From Euler's equation, $F = \frac{\pi^2 EI}{(KL)^2}$, the buckling force is proportional to the area moment of inertia, I. In our device, the cross section of the microneedle is approximately a rectangle. Thus its area moment of inertia has an exponential growth with the microneedle thickness, which was why the microneedle's buckling force changed rapidly based on its thickness. However, an overly thick microneedle can cause extensive damage to brain tissue. As a result, a 120 μm thick maltose layer was coated on the surface to increase the stiffness and reduce the invasiveness of the insertion.

3.4. Maltose dissolution testing

After achieving sufficient stiffness for tissue penetration, the next step is to ensure that the maltose on the microneedle surface can be successfully dissolved by body fluids in the tissue to expose the CNT coated contacts. As shown in figure 11, the maltose coated microneedle was capable of being inserted into a rat's brain without any deformation. After several minutes, the maltose was dissolved and cleared by the body fluids. The stiff microneedle transformed back into an ultra-thin neural probe with excellent flexibility. We subsequently studied the time taken to dissolve maltose coatings of different thickness. The testing was divided into different batches. In each batch, microneedles with the same coating thickness were inserted into a rat's brain at the same

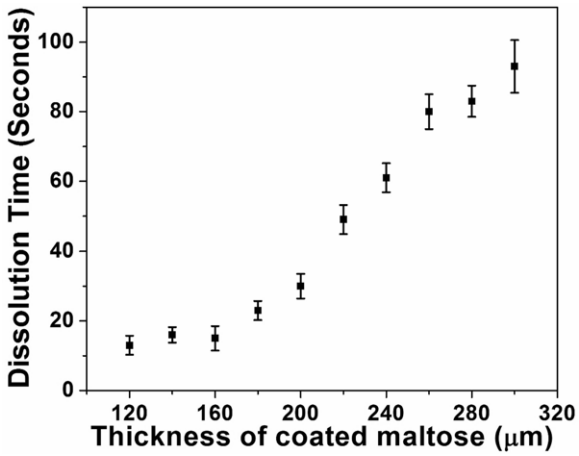

Figure 12. Means and standard error of the dissolution time for different maltose thicknesses.

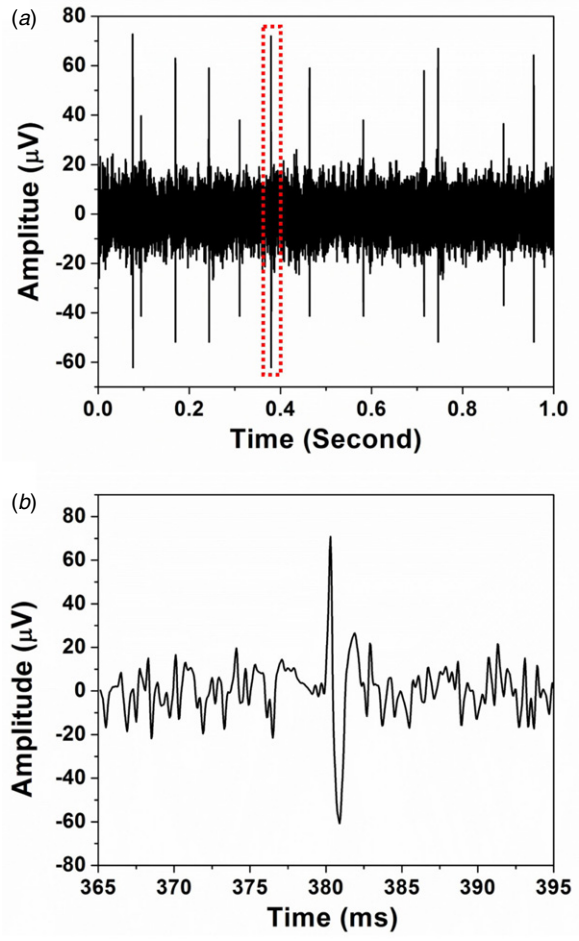

Figure 13. Neural activity recorded from the rat's dorsal hippocampus CA1 area.

time. Then these microneedles were taken out of the brain one by one with 5 s intervals. Since the maltose was mixed with methylene blue, it was straightforward to check how much of the maltose had dissolved on each of the microneedles by inspecting the color variation. The dissolution time was then determined and recorded. Thus, the approximate dissolution time for microneedles of different thicknesses was obtained (figure 12). In the figure, for thicknesses less than 180 μm, the maltose was totally dissolved in less than 20 s. However, when the thicknesses were larger than 180 μm, the dissolution time increased dramatically. It only took around 15 s for the 120 μm thick maltose coating to be dissolved. We believe that this short time period will not adversely affect a normal neurophysiology experiment.

3.5. In vivo measurements

The probe's functionality in neural recordings was tested by implanting the neural probe in the CA1 of a rat's dorsal hippocampus (2.2 mm deep). All procedures were performed under protocol 095/12(A3)13 and approved by the Institutional Animal Care and Use Committee at the National University of Singapore.

Male Sprague Dawley rats were anesthetized with pentobarbital sodium (50 mg kg^{-1}) and immobilized in a stereotaxic apparatus. A supplementary dose of 15 mg kg^{-1} h^{-1} was applied to maintain the animal under anesthesia. A craniotomy was performed posterior to the lambda landmark and a stainless steel screw was inserted to act as the ground electrode. According to [75], the position for the dorsal hippocampus CA1 area (2.0 mm lateral and 2.3 mm posterior to the bregma landmark) was located and marked. Two additional craniotomies were performed for the recording and reference electrodes. A tungsten microwire was positioned on the cortical surface to be used as the reference electrode. The maltose coated microneedle was then vertically attached to a micromanipulator located over the exposed neural tissue. Next, the probe was lowered down slowly to the CA1 area by adjusting the micromanipulator. Signals were amplified and acquired by using an RZ5D BioAmp Processor (Tucker-Davis Technologies, USA). Figure 13 shows a 1 s segment from the continuous recordings on a representative electrode contact. It showed that the spontaneous neural activity in the rat's hippocampus was successfully recorded.

4. Conclusions

This work successfully demonstrates a fabrication process to make an ultra-thin flexible polyimide neural probe. Its flexibility can minimize the problems caused by micromotion between the probe and the brain tissue. Moreover, the ultra-thin characteristic allows it to reduce the growth of the glial sheath on the body of the neural probe. In addition, maltose is first demonstrated to be suitable to coat the probe surface to transform it into a stiff microneedle temporarily during tissue penetration. The innovative drawing lithography technology is employed to provide appropriate coating uniformity and thickness. After the microneedle is implanted for several seconds, the maltose coating is shown to be dissolved by body fluids and the exposed CNT coated contacts on the neural probe are demonstrated to successfully acquire neural signals from brain tissue.

Acknowledgments

This work was supported by grants from the National Research Foundation (NRF) CRP project 'Self-Powered Body Sensor Network for Disease Management and Prevention Oriented Healthcare' (R-263-000-A27-281) and National Research Foundation (NRF) CRP project 'Peripheral Nerve Prostheses: A Paradigm Shift in Restoring Dexterous Limb Function' (R-719-000-001-281).

References

[1] Nuwer M R, Hovda D A, Schrader L M and Vespa P M 2005 Routine and quantitative EEG in mild traumatic brain injury *Clin. Neurophysiol.* **116** 2001–25

[2] Juergens E, Guettler A and Eckhorn R 1999 Visual stimulation elicits locked and induced gamma oscillations in monkey intracortical- and EEG-potentials, but not in human EEG *Exp. Brain Res.* **129** 247–59

[3] Jones M and Barth D 1999 Spatiotemporal organization of fast (>200 Hz) electrical oscillations in rat vibrissa/barrel cortex *J. Neurophysiol.* **82** 1599–609

[4] Wise K D, Angell J B and Starr A 1970 An integrated-circuit approach to extracellular microelectrodes *IEEE Trans. Biomed. Eng.* **17** 238–47

[5] Campbell P K, Jones K E, Huber R J, Horch K W and Normann R A 1991 A silicon-based, three-dimensional neural interface: manufacturing processes for an intracortical electrode array *IEEE Trans. Biomed. Eng.* **38** 758–68

[6] Cheung K, Djupsund K, Dan Y and Lee L P 2003 Implantable multichannel electrode array based on SOI technology *J. Microelectromech. Syst.* **12** 179–84

[7] Norlin P, Kindlundh M, Mouroux A, Yoshida K and Hofmann U G 2002 A 32-site neural recording probe fabricated by DRIE of SOI substrates *J. Micromech. Microeng.* **12** 414–9

[8] Yoon T H, Hwang E J, Shin D Y, Park S I, Oh S J, Jung S C, Shin H C and Kim S J 2000 A micromachined silicon depth probe for multichannel neural recording *IEEE Trans. Biomed. Eng.* **47** 1082–7

[9] Blum N A, Carkhuff B G, Charles H K, Edwards R L and Meyer R A 1991 Multisite microprobes for neural recordings *IEEE Trans. Biomed. Eng.* **38** 68–74

[10] Kuperstein M and Whittington D A 1981 A practical 24 channel microelectrode for neural recording *in vivo IEEE Trans. Biomed. Eng.* **28** 288–93

[11] Prohaska O J, Olcaytug F, Pfundner P and Dragaun H 1986 Thin-film multiple electrode probes: possibilities and limitations *IEEE Trans. Biomed. Eng.* **33** 223–9

[12] May G A, Shamma S A and White R L 1979 A tantalum-on-sapphire microelectrode array *IEEE Trans. Electron Devices* **26** 1932–9

[13] Turner J N, Shain W, Szarowski D H, Andersen M, Martins S, Isaacson M and Craighead H 1999 Cerebral astrocyte response to micromachined silicon implants *Exp. Neurol.* **156** 33–49

[14] Szarowski D H, Andersen M D, Retterer S, Spence A J, Isaacson M, Craighead H G, Turner J N and Shain W 2003 Brain responses to micro-machined silicon devices *Brain Res.* **983** 23–35

[15] Jensen W, Yoshida K and Hofmann U G 2006 *In-vivo* implant mechanics of flexible, silicon-based ACREO microelectrode arrays in rat cerebral cortex *IEEE Trans. Biomed. Eng.* **53** 934–40

[16] Biran R, Martin D C and Tresco P A 2007 The brain tissue response to implanted silicon microelectrode arrays is increased when the device is tethered to the skull *J. Biomed. Mater. Res.* A **82** 169–78

[17] Suner S, Fellows M R, Vargas-Irwin C, Nakata G K and Donoghue J P 2005 Reliability of signals from a chronically implanted, silicon-based electrode array in non-human primate primary motor cortex *IEEE Trans. Neural Syst. Rehabil. Eng.* **13** 524–41

[18] Du J, Roukes M L and Masmanidis S C 2009 Dual-side and three-dimensional microelectrode arrays fabricated from ultra-thin silicon substrates *J. Micromech. Microeng.* **19** 075008

[19] Chen C-H, Lin C-T, Hsu W-L, Chang Y-C, Yeh S-R, Li L-J and Yao D-J 2013 A flexible hydrophilic-modified graphene microprobe for neural and cardiac recording *Nanomedicine* **9** 600–4

[20] Altuna A, Gabriel G, de la Prida L M, Tijero M, Guimerá A, Berganzo J, Salido R, Villa R and Fernández L J 2010 SU-8-based microneedles for *in vitro* neural applications *J. Micromech. Microeng.* **20** 064014

[21] Tijero M, Gabriel G, Caro J, Altuna A, Hernández R, Villa R, Berganzo J, Blanco F J, Salido R and Fernández L J 2009 SU-8 microprobe with microelectrodes for monitoring electrical impedance in living tissues *Biosensors Bioelectron.* **24** 2410–6

[22] Altuna A, de la Prida L M, Bellistri E, Gabriel G, Guimerá A, Berganzo J, Villa R and Fernández L J 2012 SU-8 based microprobes with integrated planar electrodes for enhanced neural depth recording *Biosensors Bioelectron.* **37** 1–5

[23] Turner J N, Shain W, Szarowski D H, Andersen M, Martins S, Isaacson M and Craighead H 1999 Cerebral astrocyte response to micromachined silicon implants *Exp. Neurol.* **156** 33–49

[24] Li W, Rodger D C, Pinto A, Meng E, Weiland J D, Humayun M S and Tai Y C 2011 Parylene based integrated wireless single channel neurosimulator *Sensors Actuators* A **166** 193–200

[25] Kuo J T W, Kim B J, Hara S a, Lee C D, Gutierrez C a, Hoang T Q and Meng E 2013 Novel flexible parylene neural probe with 3D sheath structure for enhancing tissue integration *Lab Chip* **13** 554–61

[26] Seymour J P, Langhals N B, Anderson D J and Kipke D R 2011 Novel multi-sided, microelectrode arrays for implantable neural applications *Biomed. Microdevices* **13** 441–51

[27] Yu H, Zheng N, Wang W, Wang S, Zheng X and Li Z 2013 Electroplated nickel multielectrode microprobes with flexible parylene cable for neural recording and stimulation *J. Microelectromech. Syst.* **22** 1199–206

[28] Takeuchi S, Suzuki T, Mabuchi K and Fujita H 2004 3D flexible multichannel neural probe array *J. Micromech. Microeng.* **14** 104–7

[29] Fomani A A and Mansour R R 2011 Fabrication and characterization of the flexible neural microprobes with improved structural design *Sensors Actuators* A **168** 233–41

[30] Chen Y-Y, Lai H-Y, Lin S-H, Cho C-W, Chao W-H, Liao C-H, Tsang S, Chen Y-F and Lin S-Y 2009 Design and fabrication of a polyimide-based microelectrode array: application in neural recording and repeatable electrolytic lesion in rat brain *J. Neurosci. Methods* **182** 6–16

[31] Mercanzini A, Cheung K, Buhl D L, Boers M, Maillard A, Colin P, Bensadoun J-C, Bertsch A and Renaud P 2008 Demonstration of cortical recording using novel flexible polymer neural probes *Sensors Actuators* A **143** 90–96

[32] Tsang W M, Stone A L, Aldworth Z N, Hildebrand J G, Daniel T L, Akinwande A I and Voldman J 2010 Flexible split-ring electrode for insect flight biasing using multisite neural stimulation *IEEE Trans. Biomed. Eng.* **57** 1757–64

[33] Lee S E, Jun S B, Lee H J, Kim J, Lee S W, Im C, Shin H, Chang J W and Kim S J 2012 A flexible depth probe using

liquid crystal polymer *IEEE Trans. Biomed. Eng.* **59** 2085–94

[34] Lee K, He J, Clement R, Massia S and Kim B 2004 Biocompatible benzocyclobutene (BCB)-based neural implants with micro-fluidic channel *Biosensors Bioelectron.* **20** 404–7

[35] Polikov V S, Tresco P A and Reichert W M 2005 Response of brain tissue to chronically implanted neural electrodes *J. Neurosci. Methods* **148** 1–18

[36] Shearer M and Fawcett J 2001 The astrocyte/meningeal cell interface—a barrier to successful nerve regeneration *Cell Tissue Res.* **305** 267–73

[37] Kim Y-T, Hitchcock R W, Bridge M J and Tresco P A 2004 Chronic response of adult rat brain tissue to implants anchored to the skull *Biomaterials* **25** 2229–37

[38] Hampton D W, Rhodes K E, Zhao C, Franklin R J M and Fawcett J W 2004 The responses of oligodendrocyte precursor cells, astrocytes and microglia to a cortical stab injury, in the brain *Neuroscience* **127** 813–20

[39] Fawcett J W and Asher R 1999 The glial scar and central nervous system repair *Brain Res. Bull.* **49** 377–91

[40] Ludwig K A, Uram J D, Yang J, Martin D C and Kipke D R 2006 Chronic neural recordings using silicon microelectrode arrays electrochemically deposited with a poly(3,4-ethylenedioxythiophene) (PEDOT) film *J. Neural Eng.* **3** 59–70

[41] Johnson M D, Otto K J and Kipke D R 2005 Repeated voltage biasing improves unit recordings by reducing resistive tissue impedances *IEEE Trans. Neural Syst. Rehabil. Eng.* **13** 160–5

[42] Williams J C, Rennaker R L and Kipke D R 1999 Long-term neural recording characteristics of wire microelectrode arrays implanted in cerebral cortex *Brain Res. Protoc.* **4** 303–13

[43] Schwartz A B, Cui X T, Weber D J and Moran D W 2006 Brain-controlled interfaces: movement restoration with neural prosthetics *Neuron* **52** 205–20

[44] Rousche P J and Normann R A 1998 Chronic recording capability of the Utah intracortical electrode array in cat sensory cortex *J. Neurosci. Methods* **82** 1–15

[45] Cui X, Lee V A, Raphael Y, Wiler J A, Hetke J F, Anderson D J and Martin D C 2001 Surface modification of neural recording electrodes with conducting polymer/biomolecule blends *J. Biomed. Mater. Res.* **56** 261–72

[46] He W and Bellamkonda R V 2005 Nanoscale neuro-integrative coatings for neural implants *Biomaterials* **26** 2983–90

[47] Zhong Y and Bellamkonda R V 2005 Controlled release of anti-inflammatory agent alpha-MSH from neural implants *J. Control. Release* **106** 309–18

[48] Kim D-H and Martin D C 2006 Sustained release of dexamethasone from hydrophilic matrices using PLGA nanoparticles for neural drug delivery *Biomaterials* **27** 3031–7

[49] Shain W, Spataro L, Dilgen J, Haverstick K, Retterer S, Isaacson M, Saltzman M and Turner J N 2003 Controlling cellular reactive responses around neural prosthetic devices using peripheral and local intervention strategies *IEEE Trans. Neural Syst. Rehabil. Eng.* **11** 186–8

[50] Seymour J P and Kipke D R 2007 Neural probe design for reduced tissue encapsulation in CNS *Biomaterials* **28** 3594–607

[51] Lee K-K, He J, Singh A, Massia S, Ehteshami G, Kim B and Raupp G 2004 Polyimide-based intracortical neural implant with improved structural stiffness *J. Micromech. Microeng.* **14** 32–37

[52] Kim B J, Kuo J T W, Hara S A, Lee C D, Yu L, Gutierrez C A, Hoang T Q, Pikov V and Meng E 2013 3D parylene sheath neural probe for chronic recordings *J. Neural Eng.* **10** 045002

[53] Kozai T D Y and Kipke D R 2009 Insertion shuttle with carboxyl terminated self-assembled monolayer coatings for implanting flexible polymer neural probes in the brain *J. Neurosci. Methods* **184** 199–205

[54] Tien L W, Wu F, Tang-Schomer M D, Yoon E, Omenetto F G and Kaplan D L 2013 Silk as a multifunctional biomaterial substrate for reduced glial scarring around brain-penetrating electrodes *Adv. Funct. Mater.* **23** 3185–93

[55] Stice P, Gilletti A, Panitch A and Muthuswamy J 2007 Thin microelectrodes reduce GFAP expression in the implant site in rodent somatosensory cortex *J. Neural Eng.* **4** 42–53

[56] Chen C-H, Chuang S-C, Su H-C, Hsu W-L, Yew T-R, Chang Y-C, Yeh S-R and Yao D-J 2011 A three-dimensional flexible microprobe array for neural recording assembled through electrostatic actuation *Lab Chip* **11** 1647–55

[57] Foley C P, Nishimura N, Neeves K B, Schaffer C B and Olbricht W L 2009 Flexible microfluidic devices supported by biodegradable insertion scaffolds for convection-enhanced neural drug delivery *Biomed. Microdevices* **11** 915–24

[58] Loeb G E, Peck R A and Martyniuk J 1995 Toward the ultimate metal microelectrode *J. Neurosci. Methods* **63** 175–83

[59] Cogan S F, Guzelian A A, Agnew W F, Yuen T G H and McCreery D B 2004 Over-pulsing degrades activated iridium oxide films used for intracortical neural stimulation *J. Neurosci. Methods* **137** 141–50

[60] Keefer E W, Botterman B R, Romero M I, Rossi A F and Gross G W 2008 Carbon nanotube coating improves neuronal recordings *Nature Nanotechnol.* **3** 434–9

[61] Lu Y, Li T, Zhao X, Li M, Cao Y, Yang H and Duan Y Y 2010 Electrodeposited polypyrrole/carbon nanotubes composite films electrodes for neural interfaces *Biomaterials* **31** 5169–81

[62] Wu R-G, Yang C-S, Cheing C-C and Tseng F-G 2011 Nanocapillary electrophoretic electrochemical chip: towards analysis of biochemicals released by single cells *Interface Focus* **1** 744–53

[63] Lemmerhirt D F, Staudacher E M and Wise K D 2006 A multitransducer microsystem for insect monitoring and control *IEEE Trans. Biomed. Eng.* **53** 2084–91

[64] Fang W and Wickert J A 1996 Determining mean and gradient residual stresses in thin films using micromachined cantilevers *J. Micromech. Microeng.* **6** 301–9

[65] Metz S, Bertsch A and Renaud P 2005 Partial release and detachment of microfabricated metal and polymer structures by anodic metal dissolution *J. Microelectromech. Syst.* **14** 383–91

[66] Li C, Sauser F E, Azizkhan R G, Ahn C H and Papautsky I 2005 Polymer flip-chip bonding of pressure sensors on a flexible Kapton film for neonatal catheters *J. Micromech. Microeng.* **15** 1729–35

[67] Ulrich R, Wasef M and Im J 1999 Thermosonic gold wirebonding to electrolessly-metallized copper bondpads over benzocyclobutene *Proc. SPIE* **22** 190–5

[68] Johansson A, Janting J, Schultz P, Hoppe K, Hansen I N and Boisen A 2006 SU-8 cantilever chip interconnection *J. Micromech. Microeng.* **16** 314–9

[69] Gao B, Yue G Z, Qiu Q, Cheng Y, Shimoda H, Fleming L and Zhou O 2001 Fabrication and electron field emission properties of carbon nanotube films by electrophoretic deposition *Adv. Mater.* **13** 1770–3

[70] Xiang Z, Wang H, Pant A, Pastorin G and Lee C 2013 Development of vertical SU-8 microtubes integrated with dissolvable tips for transdermal drug delivery *Biomicrofluidics* **7** 26502

[71] Lee K, Lee H C, Lee D-S and Jung H 2010 Drawing lithography: three-dimensional fabrication of an ultrahigh-aspect-ratio microneedle *Adv. Mater.* **22** 483–6
[72] Xiang Z, Wang H, Pant A, Pastorin G and Lee C 2013 Development of vertical SU-8 microneedles for transdermal drug delivery by double drawing lithography technology *Biomicrofluidics* **7** 66501
[73] Tsang W M, Stone A L, Otten D, Aldworth Z N, Daniel T L, Hildebrand J G, Levine R B and Voldman J 2012 Insect–machine interface: a carbon nanotube-enhanced flexible neural probe *J. Neurosci. Methods* **204** 355–65
[74] Lee K, Lee C and Jung H 2011 Dissolving microneedles for transdermal drug administration prepared by stepwise controlled drawing of maltose *Biomaterials* **32** 3134–40
[75] Liu F, Jiang H, Zhong W, Wu X and Luo J 2010 Changes in ensemble activity of hippocampus CA1 neurons induced by chronic morphine administration in freely behaving mice *Neuroscience* **171** 747–59